Communication

Mechanical Behavior of Cryomilled Ni Superalloy by Spark Plasma Sintering

Z. ZHANG, B.Q. HAN, J.Y. HUANG, Y.H. HAN, Y. ZHOU, K. KAKEGAWA, and E.J. LAVERNIA

The mechanical behavior of ultra-fine-grained (UFG) INCONEL 625 superalloy prepared *via* cryomilling and spark plasma sintering (SPS) was studied. The work-hardening response of the ultra-fine-grained (600 to 700 nm) INCONEL 625 was compared to that of the material with a 1-μm grain size and the results showed normal work hardening for the latter material but not for the former. Moreover, the results suggest that a combination of high strength and good ductility can be simultaneously obtained in the UFG INCONEL 625 alloy.

DOI: 10.1007/s11661-009-9914-1

Ultra-fine-grained (UFG, 100 to 1000 nm) materials have been the subject of considerable research interest over the past two decades, in part because they represent a transitional size regime between nanostructured (*e.g.*, <100 nm) and normal micron-sized materials. Available published results show that, unlike for the conventional grain size regime in which a reduction in grain size usually leads to an increase both in strength and ductility, high strength in UFG materials is accompanied with a low ductility (frequently less than a few percent in tension).[1] Of the UFG materials that exhibit considerable ductility, an inhomogeneous microstructure (bimodal grain size distribution) is frequently reported.[2,3] For example, in bimodal Al-Mg alloys fabricated *via* cryomilling,[4,5] a true strain of 6 to 8 pct in tension was obtained. The grain size distribution in this material indicated that the fine grain size is in the range of 100 to 300 nm, whereas the coarse grains centered around 1 μm. An enhancement of ductility has also been reported for other UFG or nanostructured materials with an inhomogeneous microstructure.[6,7] The stress-strain curves of UFG materials often exhibit only a brief work-hardening region followed by nearly prefect plastic deformation. The limited ductility in UFG materials, therefore, is attributed to the lack of work hardening due to limited dislocation accumulation as a result of the small grain volume. However, in a study of INCONEL* 625 alloy,[8] normal work hardening was observed for the case of a material with a bimodal microstructure with grain sizes ranging from 200 nm to about 10 μm. A remarkable increase in strength (0.2 pct offset yield stress >1000 MPa) was also achieved in the cryomilled 625 alloy, compared to the yield strength of 379 MPa in conventionally forged 625 alloy (grain size ~200 μm). In view of these findings, the motivation of the present work is to study the grain-size-dependent work-hardening behavior in the UFG regime. These results may ultimately be implemented to establish strategies to achieve high strength and good ductility in UFG materials. In this study, UFG 625 alloy samples with different grain sizes were prepared by the spark plasma sintering (SPS) technique. To diminish the potential effect of artifacts introduced during the process (*e.g.*, porosity), compression testing is used to establish the work-hardening behavior.

Gas-atomized INCONEL 625 alloy powders (Sulzer Metco (US) Inc., Westbury, NY) were cryomilled in a liquid nitrogen environment for 8 hours with a ball-to-powder ratio 20:1. The experiment was conducted in a modified Union Process 1-S attritor (Union Process Inc., Akron, OH) at a rotation rate of 180 rpm, and more details are given in References 9 and 10. Chemical analysis of as-received and cryomilled INCONEL 625, listed in Table I, shows that the chemical composition fell within the nominal compositional range of INCONEL 625 alloy; Fe, O, N, and C, originated from the milling media, were slightly increased as a result of cryomilling.

The cryomilled 625 alloy powder was consolidated in an SPS-515S apparatus (SPS Syntex Inc., Kanagawa, Japan). Prior to consolidation, the cryomilled powder was loaded in a cylindrical graphite die with an inner diameter of 15 mm, using two graphite plungers of the same size to seal the die on both ends and transfer the load during consolidation. Then the assembly was placed in a vacuum chamber and consolidated under a pressure of 42 MPa with a low voltage (<15 V) and high-density pulsed current applied on the sample. During consolidation, the sample was first heated to a preheating temperature, 100 K below the sintering temperature, at a heating rate of ~100 K/min; then the sample was heated to the target sintering temperature at a heating rate of 33.3 K/min to avoid the sample temperature overshooting. The sintering temperature was selected to be 873, 973, 1073, 1173, and 1273 K,

*INCONEL is a trademark of INCO Alloys International, Huntington, WV.

Z. ZHANG, Postdoctoral Researcher, Y. ZHOU, Associate Researcher, and E.J. LAVERNIA, Distinguished Professor, are with the Department of Chemical Engineering and Materials Science, University of California, Davis, CA 95616. Contact e-mail: zhizhang@ucdavis.edu B.Q. HAN, formerly Assistant Researcher, Department of Chemical Engineering and Materials Science, University of California, is Senior Materials Engineer, Wood Group ESP, Inc., Oklahoma City, OK 73135. J.Y. HUANG, Principal Member of Technical Staff, is with the Center for Integrated Nanotechnologies, Sandia National Laboratories, Albuquerque, NM 87185. Y.H. HAN, formerly Research Associate, Department of Chemical Engineering and Materials Science, ,University of California, is with Pusan National University, Pusan 608-735, Korea. K. KAKEGAWA is with the Graduate School of Engineering, Chiba University, Chiba 263-8522, Japan.

Manuscript submitted April 10, 2009.
Article published online July 22, 2009

Table I. Chemical Composition (Weight Percent) of As-Received and Cryomilled INCONEL 625 Alloy Powders

Material	Ni	Cr	Mo	Nb	Ti	Al	Fe	O	N	C
As-received	bal	21.0	9.18	3.77	0.004	0.21	0.036	0.012	0.076	0.009
Cryomilled	bal	20.5	8.81	3.87	0.005	0.21	1.87	0.087	0.27	0.082
Nominal range[20]	58.0 min	20.0 to 23.0	8.0 to 10.0	3.15 to 4.15	0.40 max	0.40 max	5.0 max	—	—	0.10 max

respectively. The dwelling time at the sintering temperature was 5 minutes. The sintering temperature was monitored using a K-type thermocouple. After consolidation, the density of bulk samples was measured using Archimedes' method.

The microstructures were examined using transmission electron microscopy (TEM) and X-ray diffraction (XRD). The TEM observation was performed with a JEOL** 2010F microscope, operated at 200 kV. The TEM samples were mechanically thinned to a thickness of approximately 20 μm and then perforated using ion milling. The XRD measurements were conducted using a Scintag XDS 2000 X-ray diffractometer (Scintag Inc., Cupertino, CA) using Cu K_α radiation.

**JEOL is a trademark of Japan Electron Optics Ltd., Tokyo.

The mechanical behavior was evaluated by compression tests at ambient temperatures using an Instron 8801 universal testing machine (Instron, Canton, MA). Compression specimens were machined and tested along the loading direction of SPS, with a cubic geometry measuring approximately 5 mm per edge. The compression tests were conducted at a constant crosshead speed of 0.0005 mm/s, with measurement of the displacement of compression platens (the displacement of specimens and the elastic deformation of platens) using a video camera. The elastic strain of the compression platens was corrected.

Figure 1(a) shows the true stress-strain curves of the SPS samples consolidated, respectively, at 973, 1073, 1173, and 1273 K (designated hereafter as SPS-973, SPS-1073, SPS-1173, and SPS-1273) at a strain rate of 10^{-4} s^{-1}. The samples SPS-1273 and SPS-1173 exhibited virtually identical compression behavior. However, the sample SPS-1073 obtained a lower yield stress as well as inferior work-hardening behavior. The sample SPS-973 failed prematurely at a stress of 362 MPa. The variation of 0.2 pct offset yield stress against SPS temperature is plotted in Figure 1(b). Here, the yield stress drop in the samples SPS-973 and SPS-1073 was likely caused by the presence of porosity. Examination of the density of the SPS samples revealed that nearly full dense bulk samples (>98 pct) were achieved above 1173 K, as shown in the inset of Figure 1(b). At 973 K, the SPS sample attained a relative density of ~79 pct; at the temperature of 873 K, the SPS sintered powder did not form a solid compact. It should be mentioned that, although the SPS sintering only takes a few minutes, the SPS temperature required to achieve full density is lower than that for conventional sintering (*e.g.*, hot pressed (HP) or hot isostatic pressed (HIP)). For instance, at a sintering temperature of 1533 to 1673 K, the sintered density was reported to reach only 80 pct of theoretical density for a similar INCONEL 600 alloy.[11] In INCONEL 625 alloy consolidated using HIP, a density of 85 to 90 pct was obtained at a temperature of 1118 K.[12] Fast densification was also achieved with SPS in other material systems due to an acceleration of mass transport resulting from the presence of pulse currents.[13–18] To seal the porosity, the samples that were SPS consolidated at 1073 K were HP at 773 K (designated as SPS-HP hereafter) to full density corresponding to INCONEL 625 alloy (8.46 g/cm^3) at a deformation strain of ~8 pct (Figure 1(c)). The fully dense sample SPS-HP yielded a similar yield stress compared to the ones SPS consolidated at higher temperatures (SPS-1173 and SPS-1273), as seen in Figure 1(b). As will be discussed in a later section, the inferior working hardening rate in the sample SPS-1073 is attributed to an intrinsic characteristic of the sample.

INCONEL 625 alloy is a marginal solid-solution-strengthened alloy, and various precipitate phases may evolve at elevated temperatures; accordingly, the phase constitution in the SPS samples was identified using XRD. A solid solution formed in the as-atomized and cryomilled 625 alloy powders, as shown in Figure 2. Inspection of the XRD pattern reveals that the three peaks in each powder sample can be attributed to the (111), (200), and (220) planes of an fcc phase (γ matrix). The peaks of the γ phase shifted to higher angles with increasing SPS temperatures, indicating that the lattice parameter of the 625 alloy decreased due to precipitation of solute atoms.[19] Under thermal exposure, the solid solution decomposes and the various precipitate phases that are commonly found in the INCONEL 625 alloy are listed in Table II.[20] To determine the precipitated phases in the SPS samples, each phase listed in Table II was calculated using the program "powder cell"[21] to find a match with the peaks in the SPS samples in terms of position and intensity. Note that the C content after cryomilling is slightly higher than the typical chemistry range (0.01 to 0.04 wt pct C) in 625 alloy. As a result, the precipitation of carbides (NbC, M_6C) is the dominant precipitation reaction in the SPS samples sintered at high temperatures (>1173 K). In 625 alloy, the Al and Ti additions are maintained at a low level compared to Al-Ti hardened superalloys; hence, in general, the 625 alloy does not precipitate the γ' phase, but rather a metastable body-centered-tetragonal γ'' (Ni_3(Nb, Al, Ti)) phase or a stable orthorhombic Ni_3Nb phase (δ phase) may form as a result of the sufficient Nb addition. In the samples SPS-973 and SPS-1073, the δ phase formation is found to be the dominant precipitation reactions, whereas the metastable γ'' precipitation is not detected. Floreen *et al.*[20] pointed out that the γ'' precipitation could be markedly retarded

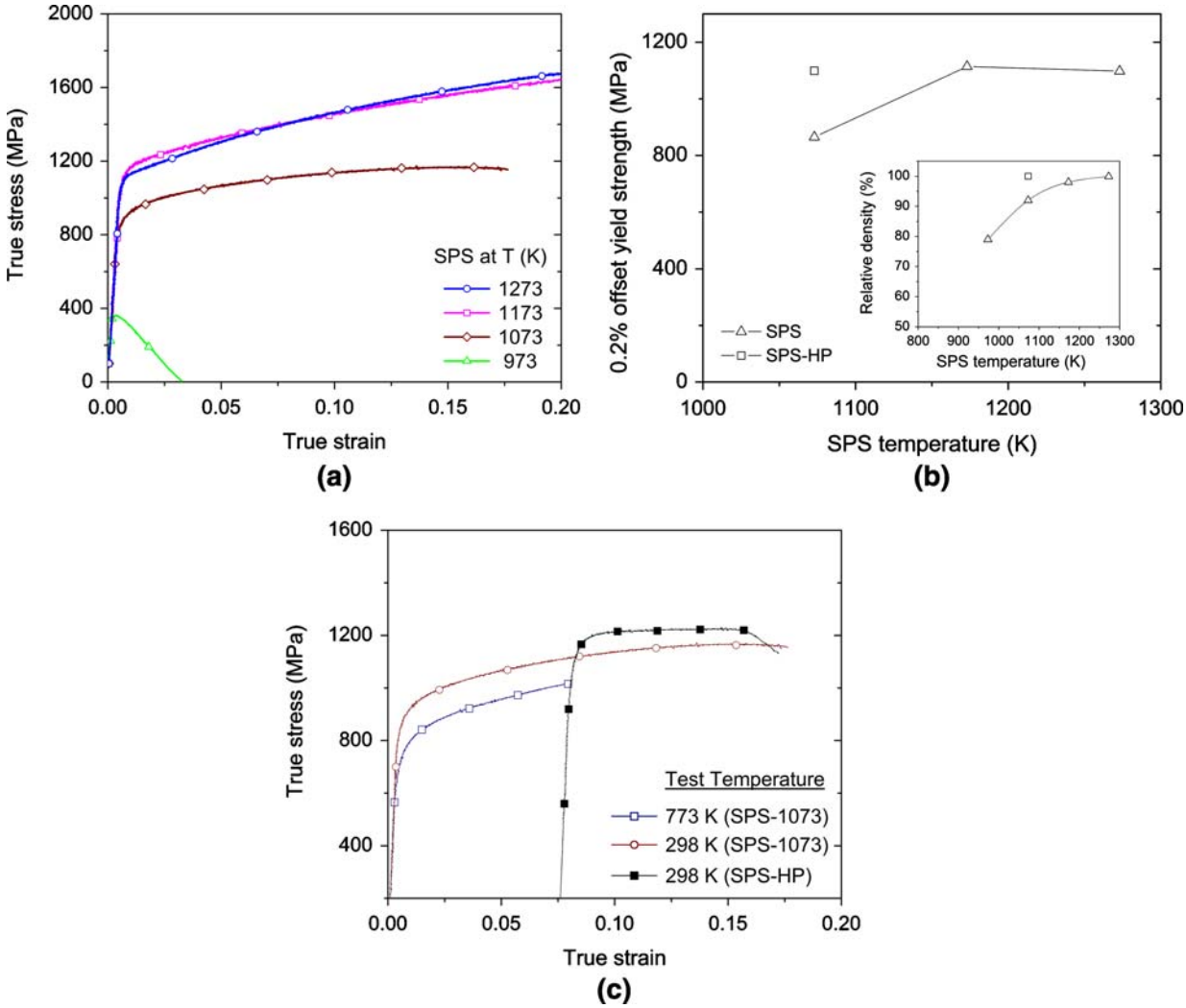

Fig. 1—(*a*) True stress-strain curves of SPS consolidated INCONEL 625 alloys. (*b*) 0.2 pct offset yield stress plotted against SPS temperature. The inset shows the variation of relative density *vs* SPS temperature. (*c*) True stress-strain behavior of sample SPS-HP.

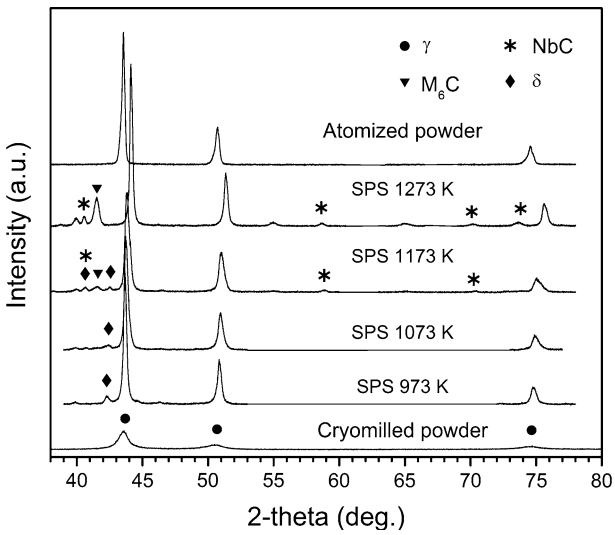

Fig. 2—XRD patterns of cryomilled INCONEL 625 alloy.

by decreasing the Ti content from 0.4 pct to 0. In the cryomilled INCONEL 625 consolidated by hot isostatic pressing, a similar observation was made on the precipitation of equilibrium δ rather than metastable γ'' phase.[8]

The microstructures of the SPS bulk samples are shown in Figure 3. Previous studies[22] indicated that the grain size in the cryomilled powder is ~30 nm. Following SPS, the grain size underwent significant growth. Most of grains in the SPS sample sintered 1073 K are approximately 600 nm, whereas some of the grains are on the order of 200 nm, as shown in Figure 3(a). The selected area electron pattern (SAED) displays the fcc pattern of γ matrix and no evidence of γ'' precipitates. The carbide and δ phase precipitates were evident in the γ matrix. With increasing SPS temperature, they precipitated preferentially from the grain boundary region to the grain interior. The grain size in the SPS sample sintered at 1173 K is on the order of 1 μm. Increasing the consolidation temperature further to 1273 K did not significantly alter the grain size, as shown in Figures 3(c)

Table II. Typical Precipitate Phases in INCONEL 625 Alloy

Phase	Crystal Structure	Composition	Precipitation Temperature (°C)	
Carbides	MC	cubic, $Fm\bar{3}m$ $a = 0.43$ nm	NbC or (Ti,Nb)C	870 to 1040
	M_6C	cubic, $Fd3m$ $a = 1.13$ nm	$(Cr,Ni,Mo)_6C$	870 to 1040
	$M_{23}C_6$	cubic, $Fm\bar{3}m$ $a = 1.08$ nm	$Cr_{23}C_6$	700 to 870
Precipitates	γ''	ord tet, $I4/mmm$ $a = 0.36$ nm, $c = 0.74$ nm	$Ni_3(Nb,Ti,Al)$	600 to 760
	δ	Orth, $Pmmn$ $a = 0.51$, $b = 0.42$, $c = 0.45$	Ni_3Nb	700 to 1000
	Laves	hex, $P6_3mmc$ $a = 0.47$ nm, $c = 0.77$ nm	$(Cr,Fe,Ni)_2(Si,Ti,Nb,Mo)$	700 to 1000
Nitrides	$(Nb,Cr)_2N$	tet, $P4/nmm$ $a = 0.3$ nm, $c = 0.77$ nm	$(Ni,Cr,Nb, Mo)_2N$	—

and (d). Smaller grains with a size of 100 to 200 nm are also observable. Twins are observed in the bulk cryomilled 625 alloy consolidated by SPS. Twin boundaries with atomic resolution are revealed by HREM, as shown in Figure 3(b). Twins were also found in cryomilled 625 alloy processed by HIP and extrusion.[8] In the as-cryomilled powder, it was found that extensive twins had formed in the nanoscale grains (grain size ~30 nm) as a result of the mechanical milling in the cryogenic temperature.[9] To determine the change of twin densities following SPS, the twin probability β, defined by finding a twin fault between the neighboring {111} planes in the fcc lattice, was calculated using the following relation: $\beta = [\Delta CG(2\theta)_{111} - \Delta CG(2\theta)_{200}]/[11\tan\theta_{111} + 14.6\tan\theta_{200}]$,[23] where θ is the diffraction angle and ΔCG is the shift of the center of gravity from peak maximum due to the peak asymmetry caused by the presence of twins, in degrees. On the basis of the measured ΔCG, the calculated twin probability in the cryomilled powder as well as the SPS samples is plotted in Figure 4. The presence of a high population of twins in the cryomilled 625 alloy powder was also revealed by TEM.[24] A high population of twins was also observed in nanostructured Ni prepared *via* cold rolling.[25] Following SPS, the XRD technique estimated that there existed two to four twins in each grain. Compared to the TEM micrograph in Figure 3, the average twin population by XRD is slightly overestimated and the XRD result appears to correspond to the twin population of the twinned grains in the SPS samples.

To compare the work-hardening behavior of the SPS samples, the dimensionless work- hardening rate $\Theta = 1/\sigma \cdot d\sigma/d\varepsilon$, which can be calculated from Figure 1(a), is plotted against strain in Figure 5(a). From Figure 5(a), the predicted uniform elongation in tension for SPS INCONEL 625 alloy can be determined by the Considère's criterion:

$$\frac{1}{\sigma}\frac{d\sigma}{d\varepsilon} = 1 \qquad [1]$$

where σ is the true stress and ε is the true strain. From Figure 5(a), letting $\Theta < 1$, we can obtain strain > 16 pct for samples SPS-1273 and SPS-1173. Hence, a uniform elongation of ~16 pct is expected prior to the onset of local necking in uniaxial tensile loading of samples SPS-1273 and SPS-1173. However, the Θ value for the sample SPS-1073 decreases more rapidly and the Θ value becomes less than 1 at a strain of 8 pct. In addition to the work-hardening rate, another material parameter used to describe the stress-strain behavior is the work-hardening exponent n. The work-hardening exponent n can be expressed by the power law (Holloman) relation:

$$\sigma = K\varepsilon^n \qquad [2]$$

where σ is the true stress, K is the strength coefficient, and ε is the true strain. The curve fitting for Eq. [2] is usually carried out in a region of uniform strain, ε_u, in tension. Here the values of ε_u for the different SPS samples are determined using Eq. [1]. Thus, the work-hardening exponent n can be determined from a plot of true stress *vs* true strain on double logarithmic scales, as shown in Figure 5(b). Note that the neck instability condition is also defined as $\varepsilon_u = n$. From Figure 5(b), the uniform strain determined from Eq. [2] is consistent with that from Eq. [1]. The work-hardening exponent n for conventionally forged INCONEL 625 alloy (grain size ~200 μm) was reported to be 0.14.[8] Figure 1(d) reveals that the n values for samples SPS-1173 and SPS-1273 are close to those of the conventionally coarse-grained counterpart, but different from the sample SPS-1073. It should be pointed out that the lower n value in sample SPS-1073 is unlikely caused by the porosity since the porosity would cause the opposite effect rather than decreasing the apparent n value in compression. This is supported by the work-hardening behavior of the fully dense SPS-HP sample. Note that although the SPS-HP sample undergoes hot deformation at 773 K in the unloading cycle, the flow stress quickly saturates at a strain of ~2 pct.

The presence of twins may also influence the strength and ductility of UFG materials. The interactions between dislocations and the twin boundaries depend on the twin lamellae thickness, twin spacing, *etc.*

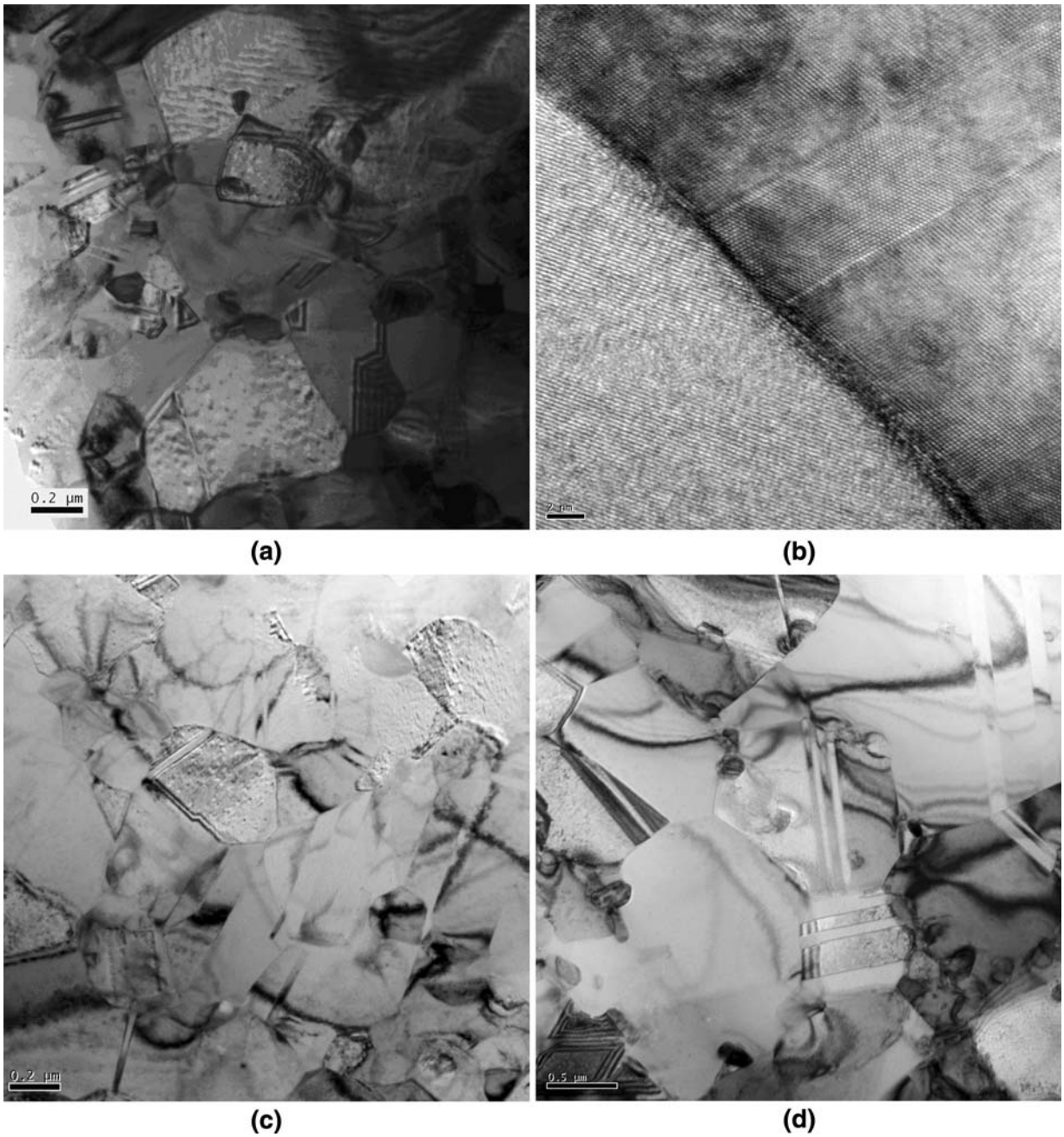

Fig. 3—Microstructures of cryomilled INCONEL alloy 625 consolidated by SPS at (*a*) and (*b*) 1073 K, (*c*) 1173 K, and (*d*) 1273 K.

Previous study[26] on UFG Cu indicated that the twins with an average spacing on the order of 90 nm did not have a significant effect on the work-hardening rate ($d\sigma/d\varepsilon$) compared to the twin-free counterpart. The twin density in the SPS samples is much lower; therefore, it can be inferred that the influence of twins in the SPS samples on the work-hardening behavior is negligible. Therefore, the grain size of ~1 μm may represent a characteristic length scale for the normal work hardening to occur. A ductility transition was also reported in Al 1100 and IF steel,[27] Al 1050,[28] and commercial purity V[29] when the grain size increased from the submicron regime to ~1 μm. However, the yield strength also decreased with increasing the grain size in these alloys. There is probably a simple explanation for the similar yield strengths of the SPS-HP, SPS-1173, and SPS-1273 samples. It is anticipated that the larger grain size in the SPS-1173 and SPS-1273 samples will decrease the yield strength, but this effect may be essentially detained by an increase in precipitate strengthening, as evidenced by the increase of the volume fraction of precipitates in the grain interior (Figures 2 and 3).

In summary, work hardening in cryomilled INCONEL 625 alloy was significantly improved by increasing the grain size from ~0.6 to ~1 μm. This study suggests an approach, based on enhancing precipitate

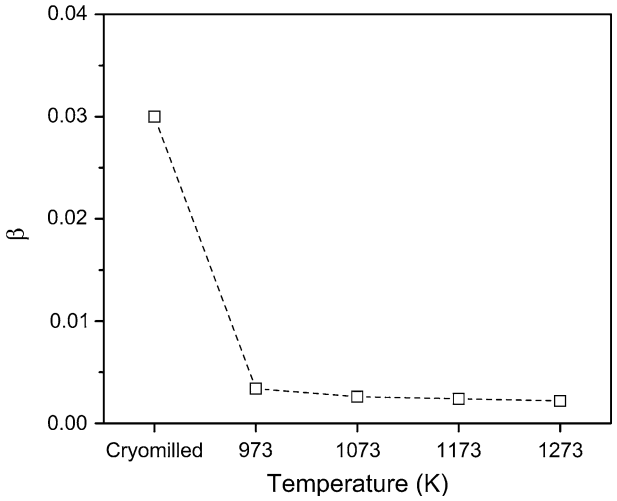

Fig. 4—Twin probability in SPS INCONEL 625 alloy.

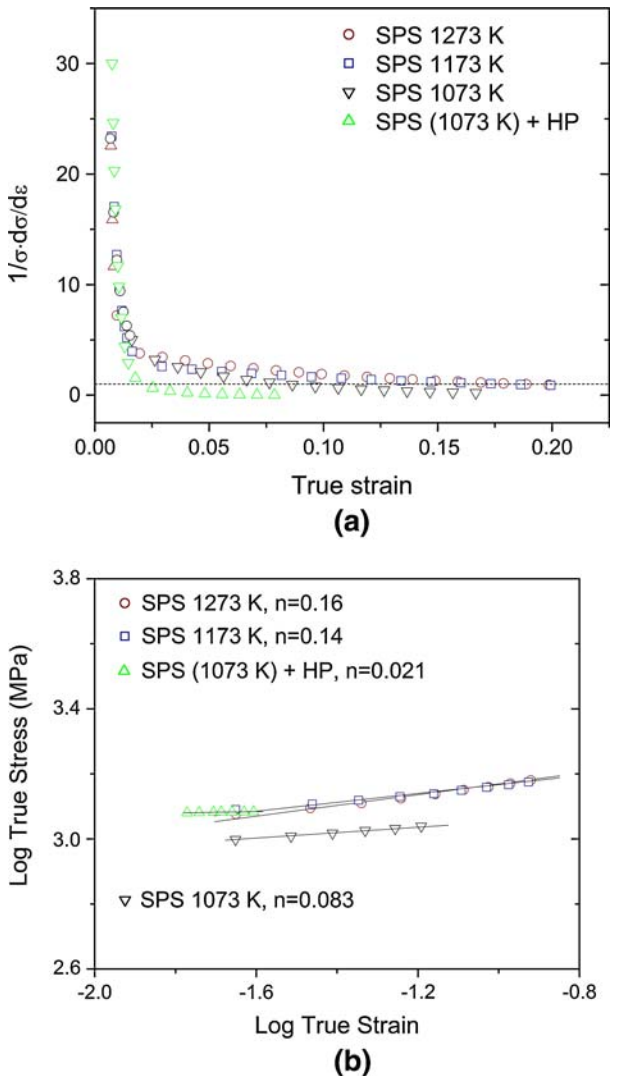

Fig. 5—(*a*) Normalized work-hardening rate as a function of strain. (*b*) True stress-strain curves on double logarithmic axes.

hardening in ~1-μm grain size, by which a combination of high strength and good ductility can be simultaneously obtained in ultra-fine-grained materials.

The authors, Z. Zhang, B.Q. Han, Y. Zhou, and E.J. Lavernia, acknowledge support by the Office of Naval Research (Grant No. N00014-1-06-0184) with Dr. Lawrence Kabacoff as program officer. J.Y. Huang acknowledges the support, in part, by the DOE Office of Basic Energy Sciences, Division of Materials Science and Engineering, and, in part, by the Center for Integrated Nanotechnologies, a DOE Office of Basic Energy Sciences user facility. Sandia National Laboratories is a multiprogram laboratory operated by Sandia Corporation, a Lockheed-Martin Company, for the United States Department of Energy under Contract No. DE-AC04-94AL85000.

OPEN ACCESS

REFERENCES

1. C.C. Koch, D.G. Morris, K. Lu, and A. Inoue: *MRS Bull.*, 1999, vol. 24, pp. 54–58.
2. M.A. Meyers, A. Mishra, and D.J. Benson: *Prog. Mater. Sci.*, 2006, vol. 51, pp. 427–56.
3. D.B. Witkin and E.J. Lavernia: *Prog. Mater. Sci.*, 2006, vol. 51, pp. 1–60.
4. D. Witkin, Z. Lee, R. Rodriguez, S. Nutt, and E. Lavernia: *Scripta Mater.*, 2003, vol. 49, pp. 297–302.
5. B.Q. Han, Z. Lee, D. Witkin, S. Nutt, and E.J. Lavernia: *Metall. Mater. Trans. A*, 2005, vol. 36A, pp. 957–65.
6. M. Legros, B.R. Elliott, M.N. Rittner, J.R. Weertman, and K.J. Hemker: *Philos. Mag. A*, 2000, vol. 80, pp. 1017–26.
7. B. Srinivasarao, K. Oh-Ishi, T. Ohkubo, T. Mukai, and K. Hono: *Scripta Mater.*, 2008, vol. 58, pp. 759–62.
8. R. Rodriguez, R.W. Hayes, P.B. Berbon, and E.J. Lavernia: *Acta Mater.*, 2003, vol. 51, pp. 911–29.
9. J.H. He and E.J. Lavernia: *J. Mater. Res.*, 2001, vol. 16, pp. 2724–32.
10. K.H. Chung, J. Lee, R. Rodriguez, D.H. Shin, and E.J. Lavernia: *Mater. Sci. Forum*, 2002, vols. 386–388, pp. 403–8.
11. D.A. Akinlade, W.F. Caley, N.L. Richards, and M.C. Chaturvedi: *Int. J. Powder Metall.*, 2006, vol. 42, pp. 43–56.
12. B.A. Hann, I. Nettleship, and S.A. Schmidt, *Superalloys 718, 625, 706 and Various Derivatives, 4th* Proc. Int. Symp., TMS, Warrendale, PA, June 15–18, 1997, pp. 781–89.
13. Z.A. Munir: *J. Mater. Synth. Proc.*, 2000, vol. 8, pp. 189–96.
14. V. Mamedov: *Powder Metall.*, 2002, vol. 45, pp. 322–28.
15. S. Paris, E. Gaffet, F. Bernard, and Z.A. Munir: *Scripta Mater.*, 2004, vol. 50, pp. 691–96.
16. H.B. Feng, Y. Zhou, D.C. Jia, and Q.C. Meng: *Mater. Sci. Eng. A*, 2005, vol. 390, pp. 344–49.
17. R. Chaim: *J. Mater. Sci.*, 2006, vol. 41, pp. 7862–71.
18. Z.J. Shen, M. Johnsson, Z. Zhao, and M. Nygren: *J. Am. Ceram. Soc.*, 2002, vol. 85, pp. 1921–27.
19. S.K. Rai, A. Kumar, V. Shankar, T. Jayakumar, K. Bhanu Sankara Rao, and B. Raj: *Scripta Mater.*, 2004, vol. 51, pp. 59–63.

20. S. Floreen, G.E. Fuchs, and W.J. Yang: *Superalloys 718, 625, 706 and Various Derivatives., 3rd Proc. Int. Symp.*, TMS, Warrendale, PA, 1994, pp. 13–37.
21. W. Kraus and G. Nolze: *J. Appl. Crystallogr.*, 1996, vol. 29, pp. 301–3.
22. K.H. Chung, J. Lee, R. Rodriguez, and E.J. Lavernia: *Metall. Mater. Trans. A*, 2002, vol. 33, pp. 125–34.
23. J.B. Cohen and C.N.J. Wagner: *J. Appl. Phys.*, 1962, vol. 33, pp. 2073–77.
24. J.H. He, K.H. Chung, X.Z. Liao, Y.T. Zhu, and E.J. Lavernia: *Metall. Mater. Trans. A*, 2003, vol. 34, pp. 707–12.
25. X.L. Wu and E. Ma: *J. Mater. Res.*, 2007, vol. 22, pp. 2241–53.
26. X.H. Chen and L. Lu: *Scripta Mater.*, 2007, vol. 57, pp. 133–36.
27. N. Tsuji, Y. Ito, Y. Saito, and Y. Minamino: *Scripta Mater.*, 2002, vol. 47, pp. 893–99.
28. C.Y. Yu, P.W. Kao, and C.P. Chang: *Acta Mater.*, 2005, vol. 53, pp. 4019–28.
29. Y.B. Chun, S.H. Ahn, D.H. Shin, and S.K. Hwang: *Mater. Sci. Eng. A*, 2009, vol. 508, pp. 253–58.